Pis'ma v ZhETF, vol. 95, iss. 4, pp. 230 – 235 © 2012 February 25

# Ab initio study of 2DEG at the surface of topological insulator $Bi_2Te_3$

*M. G. Vergniory*[+1)], *T. V. Menshchikova*[*], *S. V. Eremeev*[*×], *E. V. Chulkov*[+○]

[+] *Donostia International Physics Center, 20018 Basque Country, Spain*

[*] *Tomsk State University, 634050 Tomsk Russia*

[×] *Institute of Strength Physics and Materials Science of the Siberian Branch of the RAS, 634021 Tomks, Russia*

[○] *Departamento de Fisica de Materiales UPV/EHU, 20080 Basque Country, Spain*

Submitted 26 January 2012

By means of *ab initio* DFT-calculation we analyze the mechanism that drives the formation and evolution of the 2D electron gas (2DEG) states at the surface of $Bi_2Te_3$ topological insulator (TI). As it has been proved earlier it is due to an expansion of the van der Waals (vdW) spacing produced by intercalation of adsorbates. We will show that the effect of this expansion, in this particular surface, leads to several intriguing phenomena. On one hand we observe a different dispersion of the Dirac cone with respect to the ideal surface and the formation of Parabolic Bands (PB) below the conduction band and $M$-shaped bands in the valence band, the latters have been observed recently in photoemission experiments. On the other hand the expansion of the vdW-gaps changes the symmetry of the orbitals forming the Dirac cone and therefore producing modifications in the local spin texture. The localization of these new 2DEG-states and the relocalization of the Dirac cone will be studied as well.

Over the past few years three-dimensional topological insulators (TIs) have attracted extensive interest due to their spin-momentum-locked metallic surface states (SS) [1–5]. These kind of materials are narrow gap semiconductors characterized by an inverted energy gap caused by spin-orbit coupling (SOC). Unlike SSs in ordinary materials, these SSs show linear dispersion, forming a Dirac cone with a crossing (Dirac) point at/near the Fermi level ($E_F$) [1–3, 5]. This topological SS carries only a single electron per momentum with a spin that changes its direction consistently with a change of momentum. The topological origin of the SS protects the Dirac cone from surface perturbations [1]. The unique electronic properties of the surface of the topological insulators make these materials important for many interesting applications, particularly in spintronics and quantum computing.

Motivated by their application potential several families of TIs have been proposed theoretically and confirmed experimentally [4, 6–21]. Among them the binary layered compounds $Bi_2Se_3$, $Bi_2Te_3$, and $Sb_2Te_3$ are the most studied ones. These systems have tetradymite-like layered structure with ionic-covalent bonded quintuple layer (QL) slabs, which are linked by weak vdW forces. Such a layered structure predetermines the formation of the surface by cleavage on the vdW spacing that does not result in the formation of dangling bonds, thus only the Dirac state resides in the bulk energy gap.

[1)] e-mail: maiagv@gmail.com

However, the exploitation of the topological SS will require the interfacing of topological insulators with other materials as well as atmospheric exposure. Therefore it is essential to understand the resulting effects of the interface interaction and the possible defect/impurities migration looking at whether the topological order can survive and furthermore, whether and how the surface state may be modified under such conditions.

Recently there have been performed different experiments by ARPES where the surface of $Bi_2Se_3$ and $Bi_2Te_3$ has been studied after few hours of exposition in vacumm [22, 23], upon deposition of various magnetic [24–26] and non-magnetic [23, 25, 27] atoms and molecules as well. In the case of $Bi_2Se_3$ [22–25, 27] it has been observed a 2DEG-states formation close to the Dirac cone. These states form a parabolic band in the energy gap just bellow the conduction band and an $M$-shaped band in the local gap of bulk-projected valence band. These parabolic 2DEG-states present a large and electrostatically tunable Rashba splitting with properties far superior to any other material known before [24, 25, 28–30]. Furthermore for several adsorbates [27, 29] at the saturation deposition time a second and even a third pair of spin split parabolic states emerge below the conduction band minimum. The results in the case of $Bi_2Te_3$ are slightly different. Chen et al. [23] performed ARPES-measurements of a $Bi_2Te_3$ surface exposed to $N_2$. They reported a larger binding energy of the Dirac cone and discrete $M$-shaped

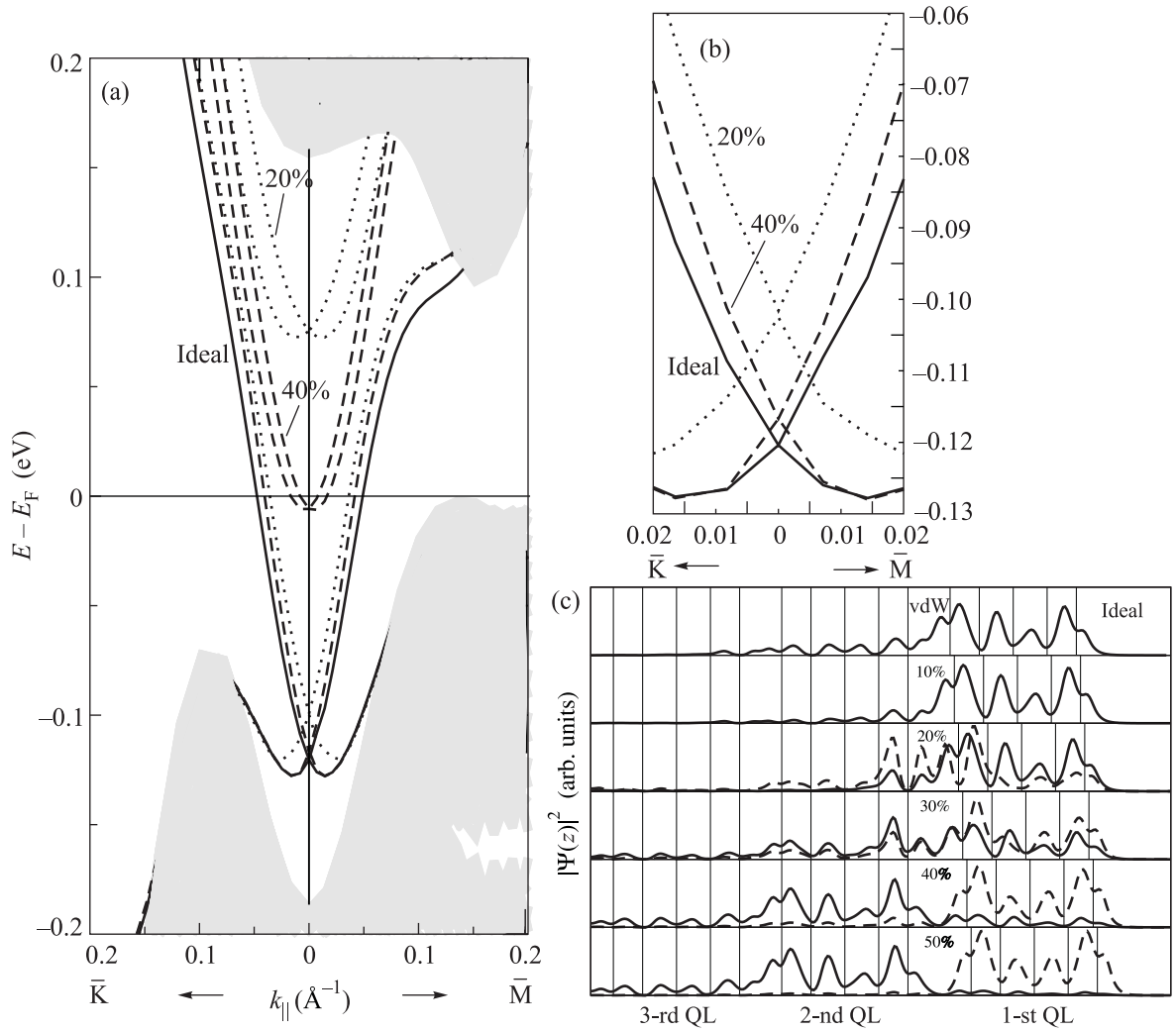


Fig. 1. (a) – Surface band structure of $Bi_2Te_3$ in the vicinity of $\bar{\Gamma}$ for an ideal case (solid line) and with the vdW-gap expanded by 20% (dotted line) and by 40% (dashed line). (b) – Dirac cone dispersions for the ideal surface (solid line), 20% expansion (dotted line) and 40% expansion (dashed line) of the vdW-gaps. (c) – Spatial localization of the topological (solid line) and parabolic (dashed line) surface states as a function of the vdW-gap expansion

bands in the top of the valence band. Another experiment on $Bi_2Te_3$ surface was carried out by Scholz et al. [26] upon Fe deposition. According to their results the Fermi energy is shifted towards higher binding energies with increasing of Fe deposition and a $M$-shaped band was resolved from 100 to 200 meV below the Dirac cone.

In recent works [31, 32] in order to understand the origin of 2DEG-states at the surface of layered topological insulators a new interpretation has been proposed: the emergence of these states is explained on the basis of a well known fact, the interlayer gaps in the layered compounds can serve as a natural containers for intercalated atoms or impurities created during the synthesis process. Various atoms are intercalated in different layered materials, inducing expansion of vdW-spacings [33]. One would expect that due to a weak binding between QLs even a relatively small concentration of contaminants in the vdW-gap can produce its sizable expansion. Performing the expansion of the vdW-gaps in $Bi_2Te_3$ we obtaine the $M$-shaped bands in the valence band reported in [23] and [26]. As an extraordinary effect we find a different dispersion of the Dirac cone for the perturbed surface with respect to the ideal surface and an upwards shifting of the energy of the Dirac point, not seen before in others compounds of the same family. We will show that for this compound we also see 2DEG-states emerging from the conduction band localized in the detached layer, as in the counterpart case of $Bi_2Se_3$. Likewise, as in the $Bi_2Se_3$ case, the expansion of various vdW-gaps produces multiple 2DEG and the localization of these states will be analyzed.

The electron band structure was calculated using DFT formalism implemented in the VASP code [34]. We employed the projector augmented-wave method [35] in order to take into account the interaction between the ion cores and valence electrons and the GGA for the exchange-correlation potential [36]. We have performed the calculations of the $Bi_2Te_3$ surface using experimental lattice parameters and optimized atomic positions of 40 layers film. To first simulate the effect of the adsorbate deposition in time as well as the impurity atom size we perform a calculation of the $Bi_2Te_3$ surface with expansion of the outermost vdW spacing by 10–50%.

**vdW-gap expansion, energy with respect to $E_F$, fitted effective mass and Rashba coupling parameter $\alpha_R$ for parabolic SS as function of the vdW expansion and position of the Dirac point with respect to the ideal case $C$**

| Expansion (%) | $E_0$ (eV) | $m^*$ $\bar{\Gamma}$-$\bar{K}$ | $m^*$ $\bar{\Gamma}$-$\bar{M}$ | $\alpha_R$ (eV·Å) $\bar{\Gamma}$-$\bar{K}$ | $\alpha_R$ (eV·Å) $\bar{\Gamma}$-$\bar{M}$ | $C$ (eV) |
|---|---|---|---|---|---|---|
| Ideal | – | – | – | – | – | 0.0 |
| 10 | – | – | – | – | – | 0.019 |
| 20 | 0.075 | 0.32 | 0.30 | 0.51 | 0.50 | 0.018 |
| 30 | 0.016 | 0.23 | 0.20 | 0.52 | 0.47 | 0.01 |
| 40 | −0.005 | 0.20 | 0.19 | 0.34 | 0.32 | 0.004 |
| 50 | −0.06 | 0.19 | 0.19 | 0.19 | 0.17 | 0.003 |

As one can see in Fig. 1a and b, the detachment of the outermost QL leads to 2 simultaneous effects: on one side we observe the emergence of the Rashba-split bands below the bottom of the bulk conduction band and on the other side we can see a displacement of the Dirac point with respect to the ideal position. The energy position of the Dirac point as well as the magnitude of the Rashba splitting parameter strongly depend on the vdW spacing expansion. At 10% the position of the Dirac point shifts upwards but no Rashba states are observed yet in the gap. Upon increasing the vdW-gap the Dirac point shifts gradually down and Rashba-split bands arise (see Table). Up to 50% expansion this also leads to the decrease of the effective mass $m^*$ of PBs and the Rashba coupling parameter $\alpha_R$ (see Table). At the same time we can see a slight $\bar{\Gamma}$-$\bar{K}$/$\bar{\Gamma}$-$\bar{M}$ anisotropy on $m^*$ for all the expansions. At 50% expansion this anisotropy disappears and the Dirac point gets closer to its ideal position.

We have also analyzed the spacial localization of the Dirac state and the PBs for all the expansions. At low expansions the emerged PBs keep a bulk-like delocalized character. This explains the obtained $\bar{\Gamma}$-$\bar{K}$/$\bar{\Gamma}$-$\bar{M}$ anisotropy that reproduces the anisotropy of the bulk states. Upon increasing the vdW spacing this state acquires more localized character and at 40–50% it almost completely lies in the detached QL (Fig. 1c). This result reproduces the behavior of $Bi_2Se_3$ [31]. The development of PB states is accompanied by a shifting of the topolog-

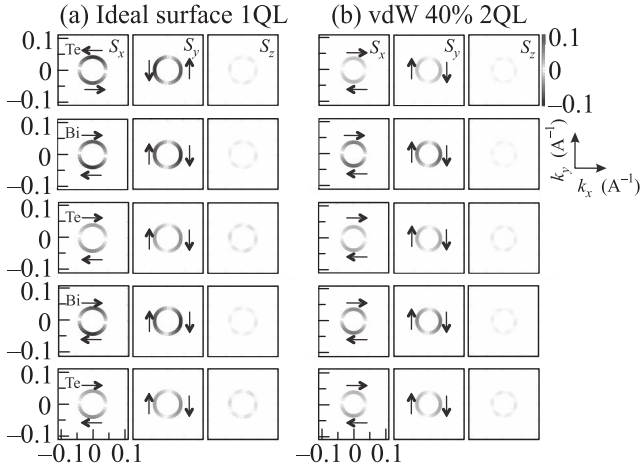


Fig. 2. Spin-resolved CEC for the topological surface state at energy of 0.1 eV above DP presented by spin projections $S_x$, $S_y$, and $S_z$ for the 1-st QL-atoms at the ideal surface (a) and for the 2-nd QL-atoms at the surface with 1-st vdW widened by 40% (b)

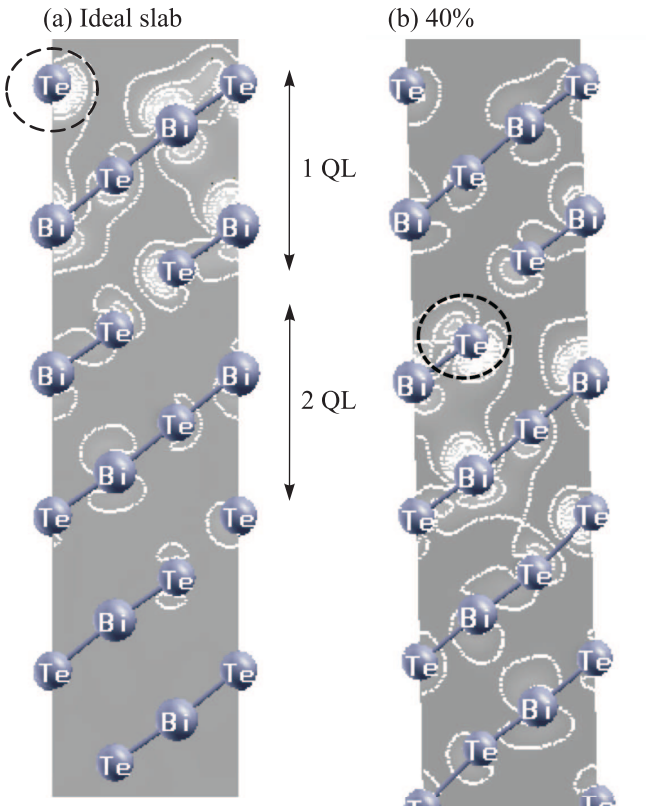


Fig. 3. Charge density distribution of the Dirac state for 0 and 40% expansion of the vdW-gap

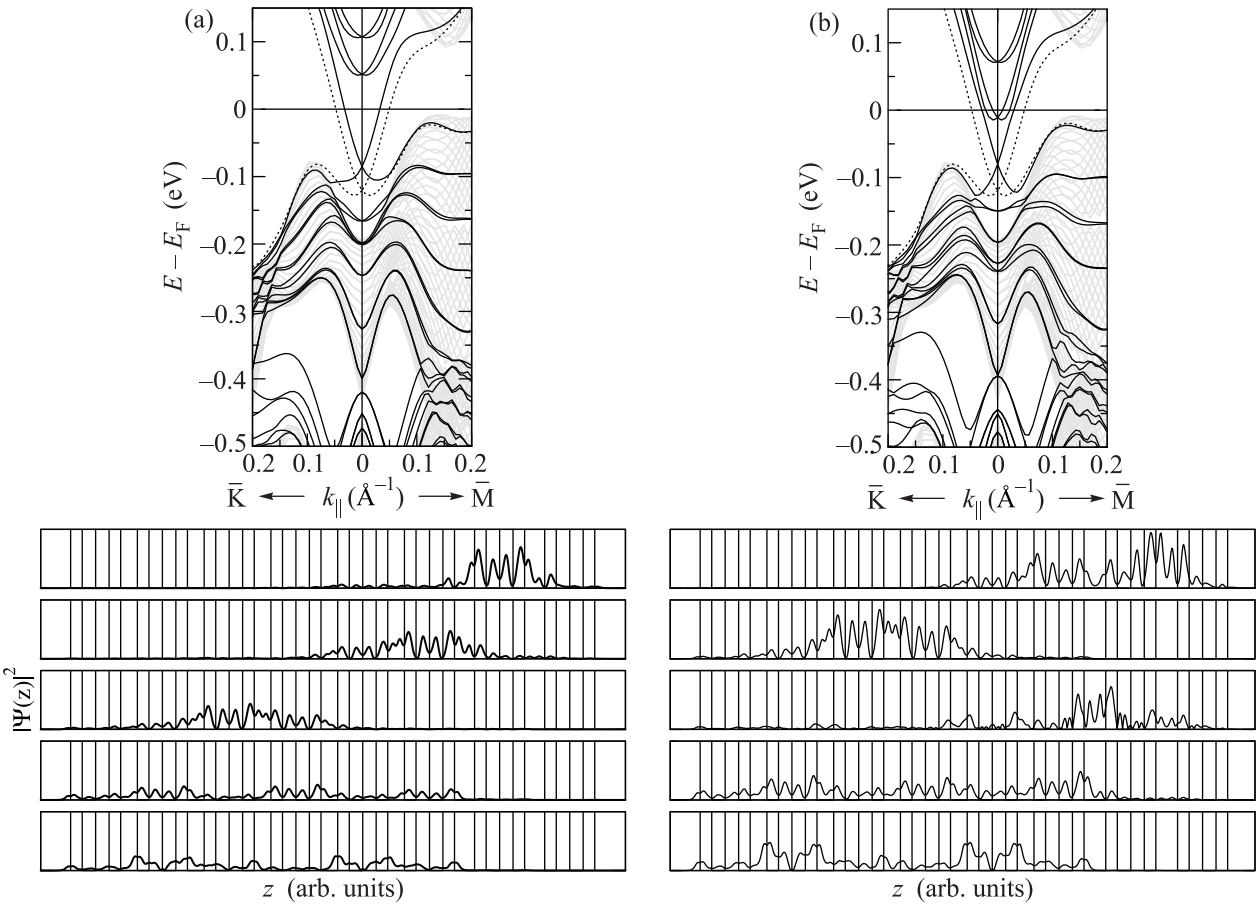


Fig. 4. Surface band structure of $Bi_2Te_3$ with the first and second vdW-gaps expanded by 20% and 20% (a), and 30% and 30% (b). The dotted line in both plots corresponds to the Dirac cone of an ideal slab. Spatial localization of each state is on the bottom part of each panels

ical state deep into the crystal, so that at 40–50% expansion the Dirac state is mostly located in the second QL, beneath the detached QL. In this case wave functions of the topological and parabolic states only slightly overlap. Nevertheless in $Bi_2Te_3$ the spatial relocation comes with the displacement of the Dirac point, contrary to what happen in the $Bi_2Se_3$, where dispersion of the upper part of the Dirac cone as well as the position of the Dirac point remain unchanged. This can be explained in terms of the localization of the Dirac state. Looking at Fig. 1c we observe that for the 20% detachment the Dirac state is more localized than in the ideal case, therefore it gets slightly higher in energy.

Next we consider the effect of relocation of the topological state on its spin texture. In Fig. 2a we can see the layer and spin-resolved constant energy contours (CEC) for the Dirac state in the topmost QL, in which the Dirac state is almost completely localized at pristine $Bi_2Te_3$ surface. As one can see, the subsurface layers have the clockwise spin rotating of the in-plane spin projections ($S_x$ and $S_y$) and weak out-of-plane spin projection $S_z$, while spin rotation in the topmost Te layer is reversed. As was shown above, the vdW-gap expansion leads to a relocation of the topological state deeper into the substrate and at 40% it is almost completely localized in the second QL. Looking at Fig. 2b we find that all layer contributions to the total spin of the Dirac state have positive (clockwise) helicity. We can attribute this alteration in the local spin texture to a change of character of the Te orbitals forming the Dirac cone. At the ideal surface the outermost Te orbitals have mostly $p_{xy}$ character (Fig. 3a), that differs from those in all other layers, where $p_{yz}$ symmetry is found. This feature can cause a change in the potential gradient that enters the spin-orbit interaction and can reverse the spin orientation in the topmost Te layer. Contrary, in the 40% vdW widening case all Te atoms of the second QL have the same $p_{yz}$ symmetry (Fig. 3b).

Now we consider the effect of simultaneous expansion of the first and second vdW-gaps. In Fig. 4a, we

show the band spectrum of $Bi_2Te_3$ with 20% expanded 1-st and 2-nd vdW spacings, respectively, and in Fig. 4b the spectrum corresponding to the same situation with 30% expansion. Similar to $Bi_2Se_3$ when detaching two vdW spacings [31] at the $Bi_2Te_3$ surface two pairs of spin-split PBs arise below the conduction bands. The most interesting feature within these two systems is the formation of $M$-shaped bands just below the Dirac point in the valence band, as distinct from $Bi_2Se_3$, where the new $M$-shaped bands arise in the valence gap. We have analyze the spacial localization of the first five bands in the valence band below the Dirac point and we find the following: if we look at Fig. 4a and b bottom panels we can observe that the first and second bands after the Dirac cone in the former case and the first and third bands in the latter case, are localized in the subsurface layers, contrary to what we find for the ideal case, were all the states in the valence band are clearly bulk states. These results reproduce well the experimental data reported by [23] and [26] where at least two bands are resolved just below the Dirac cone.

To summarize, we have analyzed the electronic structure of $Bi_2Te_3$ with the vdW-gaps widening. We have shown that for one vdW detachment we see the emergence of the Rashba-split states similar to other layered TIs. In $Bi_2Te_3$ more considerable changes in the Dirac cone at vdW expansion were found. Here, both the dispersion of the lower part of the Dirac cone and position of the Dirac point vary under the vdW expansion. Most prominent changes occur at 20% expansion and became smaller when the topological state is completely relocated into the second QL. These expansions also result in the reversion of the local spin helicity of the topological state which is linked to the difference in the symmetry of the Te atom orbitals in the first and the second QLs. We have also analyze the band structure with multiple detachments and we find new $M$-shaped bands just below the Dirac cone, reproducing the experimental data of [23] and [26]. The manipulation of these 2DEG-states has enormous potential for highly-functional spintronic applications: the control of the formation and spin splitting with external potential of these states make them a natural choice for advanced spintronic applications such as the spin-FET.

We acknowledge partial support by the University of the Basque Country (project #GV-UPV/EHU, grant #IT-366-07) and Ministerio de Ciencia e Inovación (grant #FIS2010-19609-C02-00). Calculations were performed on Arina supercomputer of the Basque Country University.

1. L. Fu and C. L. Kane, Phys. Rev. B **74**, 195312 (2006).
2. J. C. Y. Teo, L. Fu, and C. L. Kane, Phys. Rev. B **78**, 045426 (2008).
3. X. L. Qi, T. L. Hugues, and S. C. Zhang, Phys. Rev. B **78**, 195424 (2008).
4. H. Zhang, C. X. Liu, X. L. Qi et al., Nat. Phys. **78**, 076401 (2009).
5. M. Z. Hasan and C. L. Kane, Rev. Mod. Phys. **82**, 3045 (2010).
6. B. A. Bernevig, T. L. Hugues, and S. C. Zhang, Science **314**, 1757 (2006).
7. S. V. Ereemev, Y. M. Koroteev, and E. V. Chulkov, JETP Lett. **91**, 387 (2010).
8. J. H. Song, H. Jin, and A. Freeman, Phys. Rev. Lett. **105**, 096403 (2010).
9. W. Zhang, R. Yu, H. J. Zhang et al., New. J. Phys. **12**, 065013 (2010).
10. Y. Xia, D. Qian, D. Hsieh et al., Nat. Phys. **5**, 398 (2009).
11. Y. L. Chen, J. G. Analytis, J. H. Chu et al., Science **325**, 178 (2009).
12. T. Zhang, P. Cheng, X. Chen et al., Phys. Rev. Lett. **103**, 266803 (2009).
13. K. Kuroda, M. Ye, A. Kimura et al., Phys. Rev. Lett. **105**, 146801 (2010).
14. D. Xiao, Y. Yao, W. Feng et al., Phys. Rev. Lett. **105**, 096404 (2010).
15. S. Chadov, X. Qi, J. Kubler et al., Nat. Mat. **9**, 541 (2010).
16. H. Lin, L. A. Wray, Y. Xia et al., Nat. Mat. **9**, 536 (2010).
17. H. Lin, R. S. Markiewicz, L. A. Wray et al., Phys. Rev. Lett. **105**, 036404 (2010).
18. T. Sato, K. Segawa, H. Guo et al., Phys. Rev. Lett. **105**, 136802 (2010).
19. S. V. Eremeev, G. Bihlmayer, M. Vergniory et al., Phys. Rev. B **83**, 205129 (2011).
20. S. V. Eremeev, Yu. M. Koroteev, and E. V. Chulkov, JETP Lett. **92**, 161 (2011).
21. T. V. Menshchikova, S. V. Eremeev, Yu. M. Koroteev et al., JETP Lett. **93,** 15 (2010).
22. M. Bianchi, D. Guan, S. Bao et al., Nature Comm. 1:128 DOI:10.138/ncomms1131 (2010).
23. C. Chen, S. He, H. Weng et al., arXiv:1107.5784v1 (2001).
24. L. A. Wray, S. Y. Xu, Y. Xia et al., Nat. Phys. **7**, 32 (2011).
25. Z.-H. Pan, E. Vescovo, A. V. Fedorov et al., Phys. Rev. Lett. **106**, 257004 (2011).
26. M. R. Sholz, J. Sanchez-Barriga, D. Marchenko et al., arXiv:1108.1037v1 (2011).
27. L. A. Wray, S. Xu, M. Neupane et al., arXiv:1105.479v1 (2011).

28. P. D. C. King, R. C. Hatch, M. Bianchi et al., Phys. Rev. Lett. **107**, 096802 (2011).
29. Z. H. Zhu, G. Levy, B. Ludbrook et al., arXiv:1106.0552v1 (2011).
30. H. M. Benia, C. Lin, K. Kern, and C. R. Ast, Phys. Rev. Lett. **107**, 177602 (2011).
31. S. V. Eremeev, T. V. Menshchikova, M. G. Vergniory, and E. V. Chulkov, arXiv:1107.3208 (2011).
32. T. V. Menshchikova, S. V. Eremeev, and E. V. Chulkov, JETP Lett. **94**, 106 (2011).
33. R. H. Friend and A. D. Yoffe, Phys. **36**, 1 (1987).
34. G. Kresse and J. Furthmüller, Phys. Rev. B **54**, 11169 (1996).
35. G. Kresse and D. Joubert, Phys. Rev. B **59**, 1578 (1998).
36. J. P. Perdew, K. Burke, and M. Ernzerhof, Phys. Rev. Lett. **77**, 3865 (1996).